Studying Anomalous Open-Circuit Voltage Drop-Out in Concentrated Photovoltaics Using Computational Numerical Analysis

Margaret A. Stevens*, Chandler Downs*, David Emerson†, James Adler†, Scott Maclachlan‡ and Thomas E. Vandervelde *

*The Renewable Energy and Applied Photonics Labs
Tufts University, Medford, MA 02155 USA
†Department of Mathematics
Tufts University, Medford, MA 02155 USA
‡Department of Mathematics and Statistics
Memorial University, St. John's, NL, A1C 5S7, Canada

***Abstract*—Under ultra-high solar concentration, an anomalous open-circuit voltage drop-out has been observed experimentally, but not understood theoretically. This anomaly is often attributed to various thermal effects but is also observed in flash testing, where thermal effects do not have time to accumulate. As the optically generated carrier density increases past the equilibrium carrier density, open-circuit voltage and other important electrical properties could deteriorate. Using Newton linearizations and the finite-element library deal.II, we developed a computational model to solve the carrier continuity equations for optically generated charge carriers as a function of material depth in bulk III-V semiconductors.**

***Index Terms*—III-V semiconductor materials, finite element analysis, newton method, numerical simulation, photovoltaic cells.**

I. Introduction

The greatest challenge facing renewable energy is financially competing with traditionally cheap fossil fuels. Concentrating photovoltaics (CPVs) offer a route to combine high power conversion efficiencies with low costs by decreasing the illumination area needed to produce comparable power. The current record for solar cell efficiency is 46.0%, at a solar concentration of 508 suns[1]. As CPV technologies move closer to solar concentration values classified as "ultra-high" (>1000 suns), it becomes necessary to re-examine the semiconductor physics that govern our understanding of important electrical properties. By understanding the limiting behaviors of these devices, researchers will be all the more effective in designing CPV devices that can surpass the 50% conversion efficiency barrier and achieve affordability.

As shown in Figure 1, power conversion efficiency increases with solar concentration to a maximum point, but drops dramatically as concentration is increased further. This efficiency drop is most commonly attributed to the fill factor of the device, as series resistance becomes more prominent due to current flooding with high solar concentrations. Additionally, at ultra-high solar concentrations, the current generated can exceed the peak tunneling current of a multijunction device. This is suspected to have occurred to the device in Figure 1.

However, little explanation is given for the open-circuit voltage's (V_{oc}) behavior as a function of concentration. The V_{oc} of a CPV device is characterized by the following expression

$$V_{oc} = \frac{nkT}{q} ln\left(\frac{I_{sc}(X)}{I_0} + 1\right) \approx V_{oc}^{1sun} + \frac{nkT}{q} ln\,(X)\,. \tag{1}$$

Equation (1) shows that the short-circuit current (I_{sc}) is proportional to the solar concentration (X). Under high irradiance (X>100), the equation is simplified further, and V_{oc} is shown to be a function of its value at 1 sun, the diode ideality factor (n), and the solar concentration [2]. This indicates that V_{oc}, as a function of ln(X), should increase linearly, with a slope

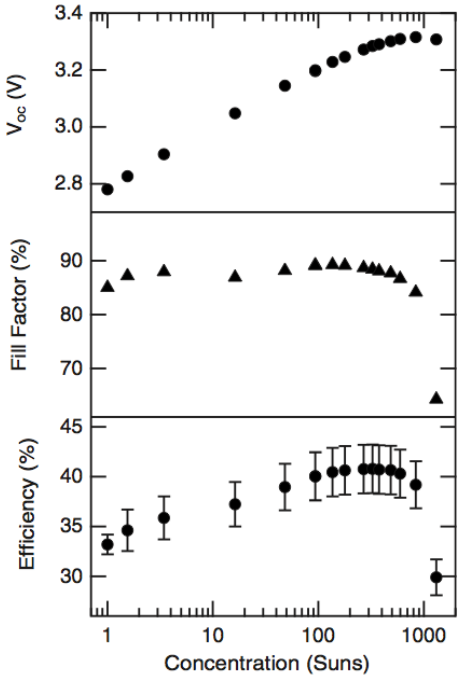

Fig. 1. Triple junction GaInP/InGaAs/InGaAs CPV subjected to high-irradiance flash testing. Voc displays anomalous drop-out [3].

determined by the diode ideality factor (n). Although this is experimentally confirmed at high irradiance, experimental data for cells subjected to ultra-high irradiance (>1000 suns) exhibits anomalous V_{oc} drop-off [2]-[6].

II. Problem Formulation

To investigate the cause of anomalous Voc drop-out in ultra-high CPVs, we employed Newton linearization and finite-element discretization to solve the carrier continuity equations without many of the standard simplifying assumptions. The total carrier density, n(x) and p(x), can be expressed as the following,

$$n(x) = n_0 + \delta n \tag{2}$$

$$p(x) = p_0 + \delta p, \tag{3}$$

which is the sum of the optically-generated charge carriers (δn and δp) and the equilibrium carriers (n_0 and p_0). Throughout this paper, we will express carrier concentrations in units of cm^{-3}. The continuity equations, defined in 1D, are as follows,

$$\frac{\partial n}{\partial t} = \frac{1}{q}\frac{\partial J_n}{\partial x} + (G - R_n) \tag{4}$$

$$\frac{\partial p}{\partial t} = -\frac{1}{q}\frac{\partial J_p}{\partial x} + (G - R_p), \tag{5}$$

where

$$J_n = qn(x)\mu_n\xi + qD_n\frac{\partial n}{\partial x} \tag{6}$$

$$J_p = qp(x)\mu_p\xi - qD_p\frac{\partial p}{\partial x}. \tag{7}$$

We solve Equation 4 when examining an n-type material, and Equation 5 when examining a p-type material. Here, μ_n and μ_p are the carrier mobilities, D_n and D_p are the carrier diffusion coefficients, ξ is the electric field in the semiconductor, G is the generation rate of carriers, and R_n and R_p are the recombination rates.

In the case of uniform doping, the equilibrium carriers can be modeled as flat distribution. Under conventional illumination, the optically generated majority carriers are orders of magnitude less than the equilibrium majority carriers, and therefore do not induce a local electric field. However, as optically generated carriers begin to overcome the equilibrium carrier density, this may not be the case. Therefore, to understand the carrier dynamics in ultra-high CPVs, we must directly solve Equations 4 and 5 for the case of high-carrier injection.

A. Recombination Term

Under low-injection conditions, the recombination rate is limited by the excess minority carriers (δn and δp), which are the optically generated in our formulation.

$$R_n = \frac{\delta n}{\tau_n} \tag{8}$$

$$R_p = \frac{\delta p}{\tau_p}. \tag{9}$$

R_n applies for a n-type material, and R_p applies for a p-type material. In the case of high-injection, as optically generated carriers increase to similar orders of magnitude as the equilibrium carriers, it will be difficult to differentiate minority and majority carriers. As a result, we propose an alternate expression for the recombination term in the carrier continuity equations.

$$R_n = R_p = \frac{\delta n(x)\delta p(x)}{\tau_p\delta n(x) + \tau_n\delta p(x)}. \tag{10}$$

In the case where $\delta n << \delta p$, this expression reduces to the low-injection R_n. In the case where $\delta p << \delta n$, this expression reduces to the low-injection R_p. When the carriers are of the same order of magnitude, and greater than the dopant concentrations ($\delta n \approx \delta p > N_D$ or N_A), this expression becomes an average of the two low-injection rates.

B. Electric Potential

Under one sun solar concentration, it is safe to assume that the optically generated carriers do not induce a local electric field. However, as the optically generated carrier densities increase towards the equilibruim carrier densities, that may not be a safe assumption. Therefore, we must solve a third equation alongside Equations 4 and 5: Poisson's Equation,

$$\nabla^2 V = -\frac{\rho}{\epsilon} \tag{11}$$

$$\frac{d^2V}{dx^2} = -\frac{q(p(x) - n(x))}{\epsilon}, \tag{12}$$

where V is the electric potential and ϵ is the relative permittivity of the material. In 1D, this simplifies to Equation 12. We can translate our computed electric potential to a local electric field by taking the derivative.

$$\xi(x) = -\frac{\mathrm{d}V}{\mathrm{d}x}. \tag{13}$$

C. Boundary Conditions

To compute the specific solutions for n(x) and p(x), we must employ 6 boundary conditions: one on each end of our material for all three quantities (n, p, and V). Assuming a chunk of semiconducting material of length L, we know that n(x) and p(x) will be constrained on the boundaries by the surface recombination rates [4]. These are Robin boundary conditions, as they constrain the value of the function and its derivative on the boundary [8].

$$n'(0) = \frac{S_r}{D_n}(n(0) - n_0) \tag{14}$$

$$n'(L) = -\frac{S_r}{D_n}(n(L) - n_0) \tag{15}$$

$$p'(0) = \frac{S_r}{D_p}(p(0) - p_0) \tag{16}$$

$$p'(L) = -\frac{S_r}{D_p}(p(L) - p_0). \tag{17}$$

S_r is the surface recombination rate. Throughout this paper, we will use prime notation to signify the spatial derivative. We

TABLE 1

Gallium Arsenide Material Parameters [7]

Electrical Properties			**Optical Properties**		
Electron Diffusion Coefficient	D_n	220 cm^2/s	Solar Concentration	X	1-10,000
Hole Diffusion Coefficient	D_p	10 cm^2/s	Photon Flux	L_{fl}	$2\times10^{17} cm^{-2}$
Electron Mobility	μ_n	8500 $cm^2/(V\cdot s)$	Reflection Coefficient	R	0.1
Hole Mobility	μ_p	400$cm^2/(V\cdot s)$	Absorption Coefficient	α	$10^5 cm^{-1}$
Carrier Lifetime	τ_n τ_p	10^{-9}sec			
Intrinsic Carrier Density	n_i	$2\times10^6 cm^{-3}$			
Relative Permittivity	ϵ	1.14×10^{-12} F/cm			
Length	L	1μm			

employed Dirichlet boundary conditions for the electric potential, since the potential difference across the semiconducting material will be known. For an intrinsic material (simplest case) we defined the potential as,

$$V(0) = 0 \tag{18}$$

$$V(L) = 0. \tag{19}$$

For a pn junction in the low-injection condition, the potential will be defined as follows,

$$V(0) = 0 \tag{20}$$

$$V(L) = \frac{kT}{q} ln\left(\frac{N_D N_A}{n_i^2}\right). \tag{21}$$

The potential difference across the device will be equal to the built-in voltage; therefore, it will be determined by the doping concentrations (N_A and N_D).

D. The Finite Element Method (FEM)

In this work, we propose a flexible computational model using Newton linearization and variational formulations, building on finite-element methods (FEM) and nested iteration to achieve numerical solutions to the carrier continuity equations [8]. Our approach derived a first-order linearization of the PDE system, allowing for discretizations and leveraging standard FEM techniques that work well for electromagnetics and fluid dynamics. We employed the Newton-Raphson method, an iterative process that finds a zero of a function in the vicinity of an initial guess, to numerically approximate the carrier concentration profiles [8]. The process is as follows,

$$0 = f'(x_k)\Delta x + f(x_k) \tag{22}$$

$$f(x_{k+1}) = f(x_k) + \Delta x. \tag{23}$$

In this work, the functions were Equations 4, 5, and 12, k was our iteration number and x_k represented the numerical approximation (n_k, p_k, and V_k in our problem). Δx represented the iterative update that moved closer to the root of the function in question.

A variational formulation of Equations 4, 5, and 12 are discretized and solved using deal.II, an open source C++ software library that facilitates solving PDE systems [9]. Integrating by parts and applying the Robin boundary conditions allowed for elimination of the second order terms, deriving a first-order variational system. The solutions, n(x) and p(x) were built using Lagrange elements of order 2, scaled to define our functions over an interval of 1 μm.

III. Results

We begin by testing our solver for the simplest case: one sun solar concentration shining on an intrinsic semiconductor in equilibrium conditions. The PDE system was as follows,

$$0 = \frac{1}{q}\frac{\partial}{\partial x}\left(qD_n\frac{\partial n(x)}{\partial x} - q\mu_n n(x)\frac{\partial V}{\partial x}\right) + G_{op} - \frac{\delta n(x)\delta p(x)}{\tau_p\delta n(x) + \tau_n\delta p(x)} \tag{24}$$

$$0 = \frac{1}{q}\frac{\partial}{\partial x}\left(qD_p\frac{\partial n(x)}{\partial x} + q\mu_p p(x)\frac{\partial V}{\partial x}\right) + G_{op} - \frac{\delta n(x)\delta p(x)}{\tau_p\delta n(x) + \tau_n\delta p(x)} \tag{25}$$

$$\frac{\partial^2 V}{\partial x} = -\frac{q\left(p(x) - n(x)\right)}{\epsilon}. \tag{26}$$

In this problem, carriers were generated by optical means; therefore, the generation rate was as follows,

$$G_{op} = \alpha X L_{fl}(1 - R)e^{-\alpha x}, \tag{27}$$

where α is the absorptivity of the material, X is the solar concentration (for 1 sun, X=1), L_{fl} is the photon flux, and R is the reflection coefficient of the material. Standard values for gallium arsenide were used for these parameters, found in Table 1.

The initial guess was comprised of an analytical solution to the carrier continuity equations when no local electric field is present. This analytical solution also employs the low-injection recombination term. When material parameters are introduced, the resulting functions for n(x) and p(x) are sums of positive and negative exponentials, added to the equilibrium concentrations.

$$n(x) = n_0 + n_1 e^{\gamma_{n1}x} + n_2 e^{-\gamma_{n2}x} + n_3 e^{-\gamma_{n3}x} \tag{28}$$

$$p(x) = p_0 + p_1 e^{\gamma_{p1}x} + p_2 e^{-\gamma_{p2}x} + p_3 e^{-\gamma_{p3}x}. \tag{29}$$

V(x)=0 was chosen for the initial guess for the electric potential as we began with a simple bulk material. Figure 2 depicts the minority carrier concentration profiles and the electric

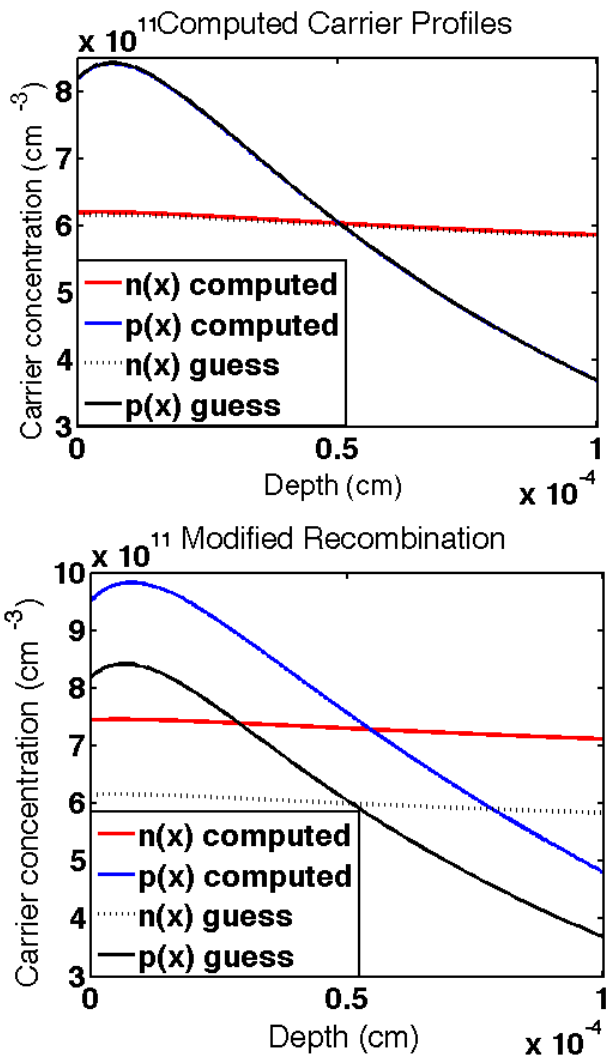

Fig. 2. Computed carrier profiles through 1μm of intrinsic GaAs. Figure (a) depicts the low-injection recombination term, while figure (b) depicts the modified recombination term proposed in this work.

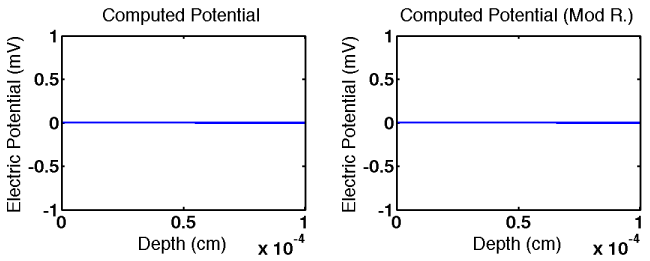

Fig. 3. Electric potential profiles through 1μm of intrinsic GaAs. Figure (a) depicts the low-injection recombination term, while figure (b) depicts the modified recombination term proposed in this work.

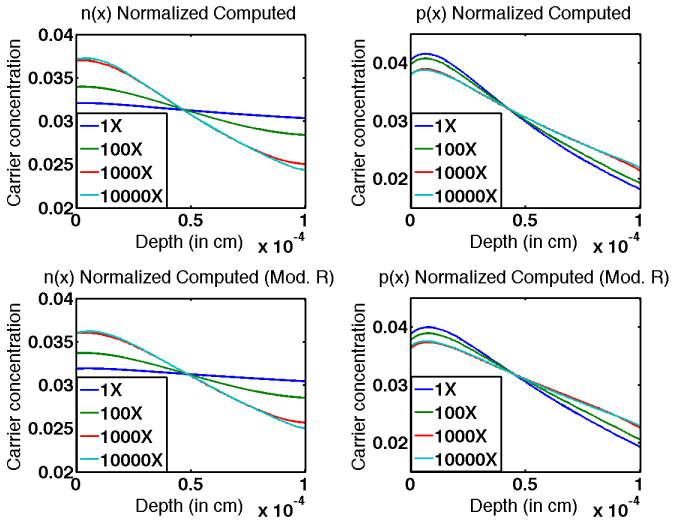

Fig. 4. Normalized plots of the computed carrier profiles with increasing solar concentration. Figures (a) and (b) depict the low-injection recombination term, while figures (c) and (d) depict the modified recombination term proposed in this work.

potential as a function of depth through 1μm of GaAs. We initially gave our solver the analytical solution computed with the low-injection recombination term and zero local electric field. As we expected, this was a stationary solution for our solver and our computed carrier profiles were nearly identical to the analytical solution. Once the accuracy of our solver was confirmed, we included the alternate recombination term. The computed solutions deviated slightly from the analytic solution, as was expected since the analytical solution employs a different recombination term, but the overall shape of the carrier density profile is unchanged. In both cases, we observed the correct electric potential solution, V(x)=0 throughout the device.

A. Increasing Concentration

As we increase the solar concentration, the minority carrier concentration profiles increase by the same orders of magnitude. However, we notice a change in the shape of the profiles as solar concentration increases. Figure 4 depicts the normalized computed carrier profiles for 4 magnitudes of solar concentration (1, 100, 1000, and 10,000 suns). As solar concentration increases, the electron concentration profile through the device steepens. The hole concentration profile seems to flatten slightly, but this profile change is much less significant than that of the electrons. We see this effect both when we implement the low-injection recombination term and when we implement the high-injection recombination term.

B. Local Electric Field

In GaAs, the electron mobility is an order of magnitude greater than the hole mobility; therefore, the electron profiles will have a more apparent change than the holes. As mentioned previously, when an analytic solution for excess carriers in a device is directly solved, one must assume negligible drift current (no local electric field) within the device. The analytic solution's PDE system was as follows,

$$0 = \frac{D_n}{q}\frac{\partial^2 n(x)}{\partial x} + G_{op} - \frac{\delta n(x)}{\tau_n} \tag{30}$$

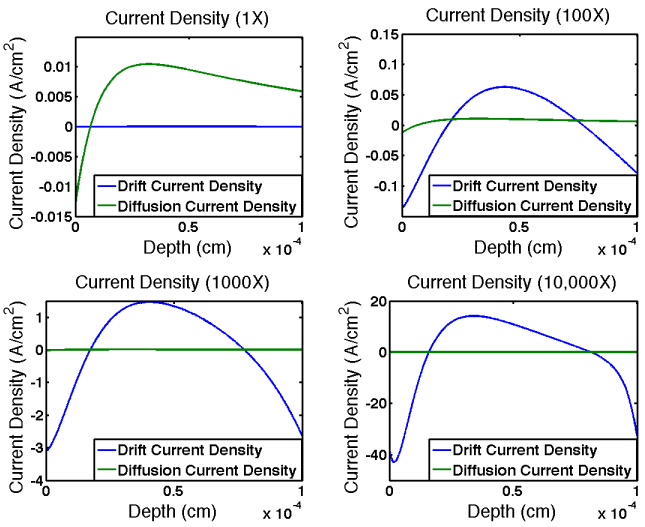

Fig. 5. Plots of drift and diffusion current as a function of depth through 1μm of intrinsic GaAs. At low solar concentrations, drift current is negligible compared to diffusion current. At high concentrations, this is not the case.

$$0 = \frac{D_p}{q}\frac{\partial^2 p(x)}{\partial x} + G_{op} - \frac{\delta p(x)}{\tau_p}, \tag{31}$$

with boundary conditions given by Equations 14-17.

While this is a safe assumption for 1 sun solar concentration, the solver shows that this assumption breaks down at higher concentrations. Figure 5 depicts the drift and diffusion currents as a function of depth in the bulk material for the same solar illuminations as shown in Figure 4 (1, 100, 1000, 10,000 suns). As solar concentration increases, the drift current is no longer negligible, and must be accounted for in the carrier continuity equations. We believe that the solver can more accurately solve for the carrier profiles at high concentrations as it incorporates the drift current and the electric field.

IV. Summary

In this work, we have explored methods of solving a nonlinear PDE system that governs the spatial dependence of electrons and holes in ultra-high concentration photovoltaics. Using the deal.II finite-element library, we successfully solved the carrier continuity equations for optically generated charge carriers in GaAs under various solar concentrations. We have shown that typical methods of characterizing excess carrier profiles cannot apply under high irradiance, ultimately impacting our understanding of electrical properties such as open-circuit voltage. In future work, we will apply deal.II using ultra-high concentration parameters in a dynamic, rather than quasi-steady state, case. Ultimately, we will use these carrier concentration profiles to electrically model CPV devices.

Acknowledgments

This work is supported by the NSF (NSF-ECCS 1055203) and the Tufts Collaborates Seed Grant Program.

References

[1] M. A. Green, K. Emery, Y. Hishikawa, W. Warta, and E. D. Dunlop, "Solar cell efficiency tables (Version 45)", *Progress in Photovoltaics: Research and Applications*, vol. 23, pp. 19, 2014.

[2] A. Vossier, D. Chemisana, G. Flamant, and A. Dollet,"Very high fluxes for concentrating photovoltaics: considerations from simple experiments and modeling *Renewable Energy*, vol. 38(1), pp 31-39, 2012.

[3] J. F. Geisz, D. J. Friedman, J. S. Ward, A. Duda, W. J. Olavarria et al., "40.8% efficient inverted triple-junction solar cell with two independently metamorphic junctions *Applied Physics Letters*, vol. 93(1), 123505, 2008.

[4] S. M. Sze and K. K. Ng, *Physics of Semiconductor Devices* 3rd ed. New York, NY: Wiley, 2006.

[5] A. Braun, B. Hirsch, A. Vossier, E. A. Katz, J. M. Gordon,"Temperature dynamics of multijunction concentrator solar cells up to ultra-high irradiance *Progress in Photovoltaics: Research and Applications*, vol. 21, pp. 202-208, 2013.

[6] A. Vossier, B. Hirsch, J. M. Gordon, "Is Auger recombination the ultimate performance limiter in concentrator solar cells? *Applied Physics Letters*, vol. 97, 193509, 2010.

[7] C. Downs *Phenomena and Performance of High Efficiency Split Spectrum Photovoltaics* Ph.D. Thesis. Tufts University: USA, 2014.

[8] S. C. Brenner and R. Scott, *The Mathematical Theory of Finite Element Methods* 3rd ed. New York, NY: Springer, 2008.

[9] W. Bangerth, R. Hartmann, G. Kanschat, "deal.II- A General-Purpose Object-Oriented Finite Element Library" *ACM Trans. Math. Softw.* 33, (4) (2007) 24/1-24/27